Materials Today: Proceedings xxx (xxxx) xxx

Contents lists available at ScienceDirect

Materials Today: Proceedings

journal homepage: www.elsevier.com/locate/matpr

Effects of cell orientation on compressive behaviour of electron beam powder bed fusion Ti6Al4V lattice structures

Y. Huang [a], A.R.O. Wan [a], K. Schmidt [b], P. Sefont [b], S. Singamneni [a], Z.W. Chen [a,*]

[a] Department of Mechanical Engineering, Auckland University of Technology, Auckland 1010, New Zealand
[b] Zenith Tecnica, Auckland 0632, New Zealand

ARTICLE INFO

Article history:
Available online xxxx

Keywords:
Build orientation
Strut irregularity
Strength
Failure
Anisotropy

ABSTRACT

Electron beam powder bed fusion (EBPBF) is suitable for making porous (or lattice) structures for medical implant applications. However, it is challenging for a lattice structure with a high porosity level to have sufficient strength, while lattice structures with sufficient strength are required for orthopedic applications. Furthermore, strength anisotropy needs to be understood for the design of femoral stems as load direction (LD) is location dependent. The present study aims to understand the effects of cell orientation on the compressive behavior of simple cubic lattice structures built using EBPBF and Ti6Al4V alloy, with [0 0 1]//LD or [1 1 1]//LD. It has been found that the apparent yield strength ($\sigma_{y\text{-}L}$) of [0 0 1] lattices is 1.8 times higher than that of [1 1 1] lattices, by experimental determination and also by numerical simulation. Simulation has shown that, with the [0 0 1]//LD condition, σ_1 in vertical load supporting struts is low when the structure yields. But locally, σ_1 (>1,000 MPa) is positive and high for the [1 1 1]/LD condition when yielding of the structure occurs with the load value only 57% of the value that is required for causing yielding in the [0 0 1]//LD condition. The predictive yield strength values by simulation of both [0 0 1] and [1 1 1] lattices have been found to be slightly lower than the experimentally determined values. Explanation for this will be provided by considering the effect of the struct effective diameter with EBPBF strut irregularity on the strength of the lattice structures.

1. Introduction

Powder bed fusion (either laser based, LPBF, or electron beam based, EBPBF) metal additive manufacturing process allows for parts with highly complex shapes to be produced. Thus, utilizing PBF to build lattice structures aiming for biomedical/implants applications has been extensively explored in recent years [1]. Porous structures with 0.3–0.6 mm pore sizes can be produced using PBF for the function of osseointegration and osteoconduction required for orthopedic implants are well understood [2]. For this reason, PBF is increasingly being applied for manufacturing metallic lattice structures [2,3]. The other necessary function of many implants is to suitably support the required loading. Thus, mechanical properties of PBF lattice structures have been extensively studied and tested. Compression loading is more dominant in biomedical implant applications and compressive tests are more widely used.

Further to the yield strength ($\sigma_{Y\text{-}L}$) and ultimate compression strength (UCS_L) of lattice structures, elastic modulus (E_L) is very important, since lattice structures as implants need to match bones in elastic modulus for not causing stress shielding. For PBF (both LPBF [4,5] and EBPBF [6,7]) lattices, E_L/E_S and $\sigma_{Y\text{-}L}/\sigma_{Y\text{-}S}$ (and UCS_L/UCS_S) is proportional to $(\rho_L/\rho_S)^{n1}$ and $(\rho_L/\rho_S)^{n2}$, respectively, as proposed by Gibson and Ashby [8], where subscript S signifies solid, ρ is density and n1 and n2 are power constants. In the studies that have been reviewed by Zhang et al. [6] and Horn et al. [9] and the further tests conducted by Del Guercio et al. [10,11] on EBPBF Ti6Al4V lattices, how loading in various directions of the lattice samples or how the build direction of EBPBF may affect E_L/E_S or $\sigma_{Y\text{-}L}/\sigma_{Y\text{-}S}$ (and UCS_L/UCS_S) has not been considered.

For biomedical implant applications, although implants are dominantly subject to axial compression, the actual loading can be in various directions. Thus, whether the mechanical properties are loading and/or build orientation dependent need to be under-

* Corresponding author.
E-mail address: zhan.chen@aut.ac.nz (Z.W. Chen).

https://doi.org/10.1016/j.matpr.2023.04.522
2214-7853/

stood. In the present study, lattices with simple cubic unit cells were EBPBF-built with two different orientations in relation to build direction (BD) which is the same as loading direction (LD) during compression testing. One was the commonly used with the unit cell [001] parallel to BD, meaning [001]//BD, and the other was [111]//BD. Samples were built with ρ_L/ρ_S = 0.36 in design which is a typical value for implant applications with ρ_L = 1.6 g/cm^3, close to the density of human femur cortical bone (1.85 g/cm^3). Compression tests were conducted to determine the effects of unit cell orientation on the strength and on the modulus of the lattices. Evaluation has been made taking into consideration of EBPBF strut irregularity, and finite element simulation has been conducted to aid the understanding of the tested data obtained.

2. Experimental procedures

Test samples were made using the commonly used EBPBF Ti6Al4V alloy powder and were produced using an Arcam Q10 EBM machine in a standard EBPBF theme for lattice structures. Lattices with simple cubic unit cells were built and either [001] or [111], respectively, is parallel to BD during EBPBF. The designed cell size was 1.1 mm × 1.1 mm × 1.1 mm and the designed strut size was 0.5 mm, giving ρ_L/ρ_S = 0.36. The two orientations are illustrated in Fig. 1a. A unit cell with [001] parallel to BD is drawn (black). For [111] lattice samples, the original unit cell is rotated about [1 $\bar{1}$ 0] for 54.7° so that [111] becomes parallel to BD ([111] unit cell is not drawn in Fig. 1). As illustrated in Fig. 1b, in a [001] cell, there is only one major load supporting vertical strut at each node, while three struts support the load at each corner in [111]. Fig. 1c shows one each of [001]//LD and [111]/LD built samples. The nominal size of the lattice portion of a sample is approximately 20 mm in height and 10 mm in diameter. Both ends of a sample are fully solid to ensure that the deformation should almost solely be in the lattice section during testing.

Compression testing was conducted using a Tinius Olsen H50KS tester in compression mode with a crosshead moving speed of 1.2 mm/min. Crosshead displacement and load were recorded during a test and apparent E_L, $\sigma_{y\text{-}L}$ and UCS_L determined from the force and extension curves of compression tests based on the nominal 10 mm diameter and the nominal "gauge" length of 20 mm which is the length of the lattice portion of the samples. The as-built and tested samples were examined using a Hitachi SU-70 scanning electron microscope (SEM). Effective strut diameters of samples were estimated. This was done by applying image analysis on SEM images using ImageJ software.

In addition, the 3D models of the lattice structures with an overall dimension of diameter ∅ = 10 mm and height h = 20 mm were constructed in the computer-aided-design package SolidWorks, and the numerical simulation was carried out using the commercial tool ANSYS Mechanical employing the finite element (FE) method. The bi-linear elastic–plastic material properties of solid Ti-6Al-4V alloy were used. A top and a bottom circular plate are bonded together with the lattice for applying the boundary conditions. A fixed boundary condition was applied at the bottom plate, while an axial displacement boundary condition was applied to the top plate. The mesh sensitivity analysis was performed, giving that the mesh size of 0.2 mm is appropriate for this study. Then the strain–stress curves were obtained to calculate E_L and $\sigma_{y\text{-}L}$ (0.2% yield stress) of the lattices.

3. Results and discussion

3.1. Experimental and simulated E_L, $\sigma_{y\text{-}L}$ and UCS_L

Three stress–strain curves for [001] lattices and also three curves for [111] lattices are shown in Fig. 2, together with the respective simulated curve. For [001] lattices, each test stopped slightly after UCS_L was reached. In these tests, samples did not collapse when UCS_L was reached but the lattice samples could be seen to have started distorting. In each of the tests of [111] lattice samples, soon after UCS_L was reached, the sample collapsed by fracturing of struts quite quickly and largely along to a plane of struts. As is clear in Fig. 2b, for two [111] lattice sample tests, the test was stopped soon after UCS_L was reached and the sample has collapsed, but for one, test continued well after the first lattice collapse (red curve). From all the curves in Fig. 2, E_L, $\sigma_{y\text{-}L}$ and UCS_L values have been determined and listed in Table 1. The test results are quite reproducible as suggested by the low standard deviation values.

Both experimental and simulative determination show $E_{L\text{-}[001]}$ is significantly higher than $E_{L\text{-}[111]}$ but $E_{L\text{-}[001]}/E_{L\text{-}[111]}$ from experiments differs from that predicted by simulation. Note that, as strain-gauge to measure the gauge length displacement cannot be used, more precise E_L values cannot be obtained. The important

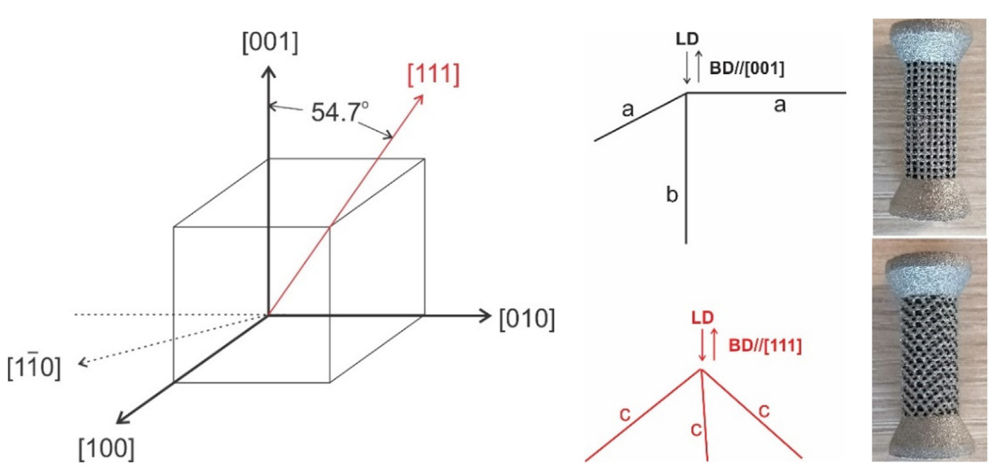

a. b. c.

Fig. 1. Illustration of EBPBF simple cubic samples: (a) unit cell (drawn black) with [001] parallel to BD and unit cell [111] (drawn red) to rotate about [1$\bar{1}$0] for 54.7° to be parallel to BD (b) the three struts jointing in a corner relative to BD (thus LD) for the two different orientated lattices and (c) an EBPBF sample each of [001] and [111] lattices. (For interpretation of the references to colour in this figure legend, the reader is referred to the web version of this article.)

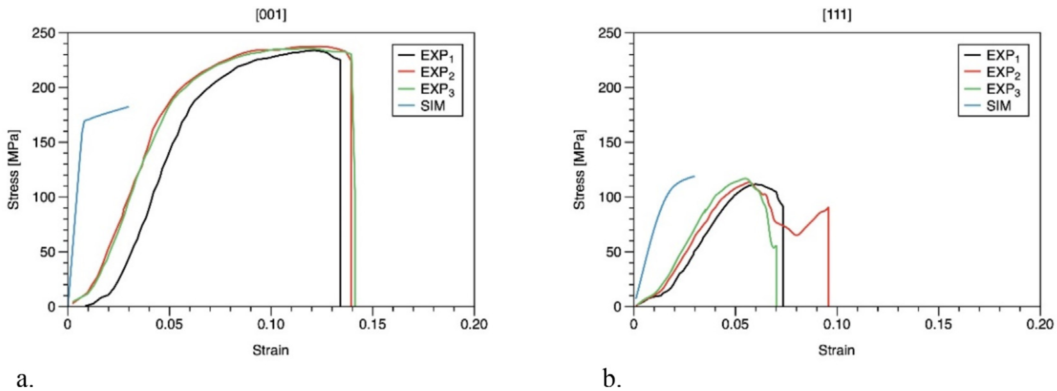

Fig. 2. Simulated (SIM)) and compressive strain–stress test (EXP) curves of (a) [001] and (b) [111] lattice samples.

Table 1
Experimentally determined (with one standard deviation values) and simulated compressive property values.

Lattice	Experiment				Simulation	
	E_L, GPa	$\sigma_{y\text{-}L}$, MPa	UCS_L, MPa	ε_p	E, GPa	$\sigma_{y\text{-}L}$, MPa
[001]	4.7 ± 0.1	189 ± 5	237 ± 1	0.065 ± 0.005	23.1	172
[111]	3.0 ± 0.2	105 ± 0	114 ± 2	0.011 ± 0.001	7.4	98
	$E_{L[001]}/E_{L[111]}$	$\sigma_{y\text{-}L[001]}/\sigma_{y\text{-}L[111]}$	$UCS_{L[001]}$ $UCS_{L[111]}$	$\varepsilon_{p[001]}/\varepsilon_{p[111]}$	$E_{L[001]}/E_{L[111]}$	$\sigma_{y\text{-}L[001]}/\sigma_{y\text{-}L[111]}$
[001]/[111]	1.6	1.8	2.1	5.9	3.1	1.8

feature from the test data is that $\sigma_{y\text{-}L}$ and UCS_L of [001] lattices is 1.8 times and 2.1 times, respectively, higher than $\sigma_{y\text{-}L}$ and UCS_L of [111] lattices. The ratio, $\sigma_{y\text{-}L[001]}/\sigma_{y\text{-}L[111]}$ being 1.8 from experiments is agreeable with that predicted by simulation. Two further features are also clear in the test curves in Fig. 2 and from the values listed in Table 1. The first (further Feature 1) relates to the comparison between the strength values experimentally determined from the test curves and values from simulation. Experimental $\sigma_{y\text{-}L[001]}$ is ~10% higher and $\sigma_{y\text{-}L[111]}$ is ~7% higher than the values from simulation. The second (further Feature 2) is the difference in the plastic strain (ε_p) corresponding to UCS_L and $\varepsilon_{p[001]}$ being 0.065, is 5.9 times of $\varepsilon_{p[001]}$ which is very low at 0.011. In the next section, strut irregularity and stress concentration are considered to explain the two further features.

3.2. Effects of EBPBF strut irregularity and stress distribution on lattice strength

Fig. 3 shows the SEM images of a [001] lattice sample. It can be clearly seen that the struts of the sample are highly irregular and highly rough, locally with notches and bumps. The major contributing factor for this is the powder particles on side surfaces of the part being partially melted during EBPBF. As the powder size on average is ~70 μm and the design strut diameter (d_{des}) is 0.5 mm, the maximum strut diameter should thus reach at least 0.64 mm. On the other hand, the small strut size (0.5 mm) and the scan (printing) needing almost point melting layer by layer means low variation of strut diameter being difficult to achieve. The SEM images were analysed using ImageJ to trace the strut shape, as indicated in Fig. 3, and the strut size was measured using a Python code. Measurement was based on a total number of 20 randomly selected struts of the [001] lattice, giving the average strut diameter d_{avg} = 0.63 ± 0.03 mm (the error being one standard deviation). The actual d_{avg} significantly higher than d_{des} may explain, referring to further Feature 1, why the experimentally determined $\sigma_{y\text{-}L}$ is higher than $\sigma_{y\text{-}L}$ predicted from simulation using d_{des} = 0.5 mm.

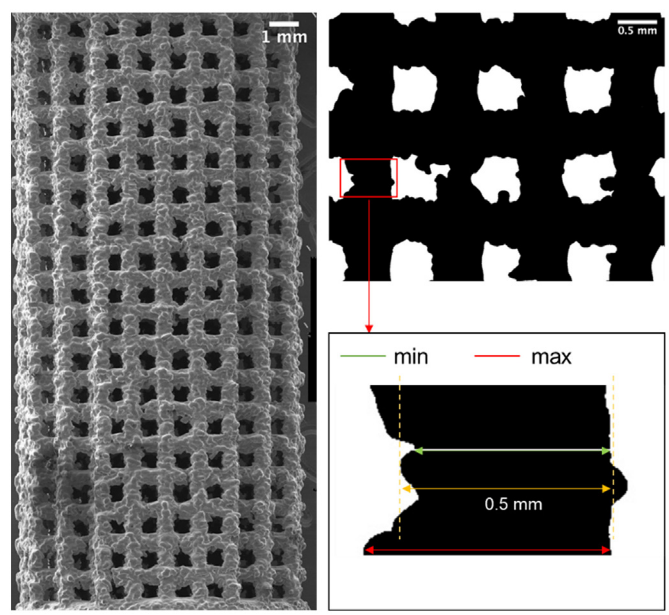

Fig. 3. SEM images of an EBPBF [001] lattice sample on the left and on the right Image-J images after setting the appropriate threshold value of local cells and a strut indicating how the strut size is measured.

The strut irregularity may have another effect on [001] lattices in Fig. 2a, referring to the apparent work hardening of the lattices. For the simulated curve, a Tangent Modulus ($E_t = d\sigma/d\varepsilon$ = 1,332 MPa) of solid Ti6Al4V in plastic region was used. For [001] lattices, $d\sigma/d\varepsilon \approx$ 580 MPa after the yield point in the simulation curve, while $d\sigma/d\varepsilon \approx$ 2,300 MPa in the experimental curves. During the test of a sample with a varying strut diameter, deformation of struts cannot be uniform. Plastic deformation should start first at the location of smallest diameter, with a notch. The continuous compressive deformation then results in the plastically deformed location becoming larger in diameter, while at other locations,

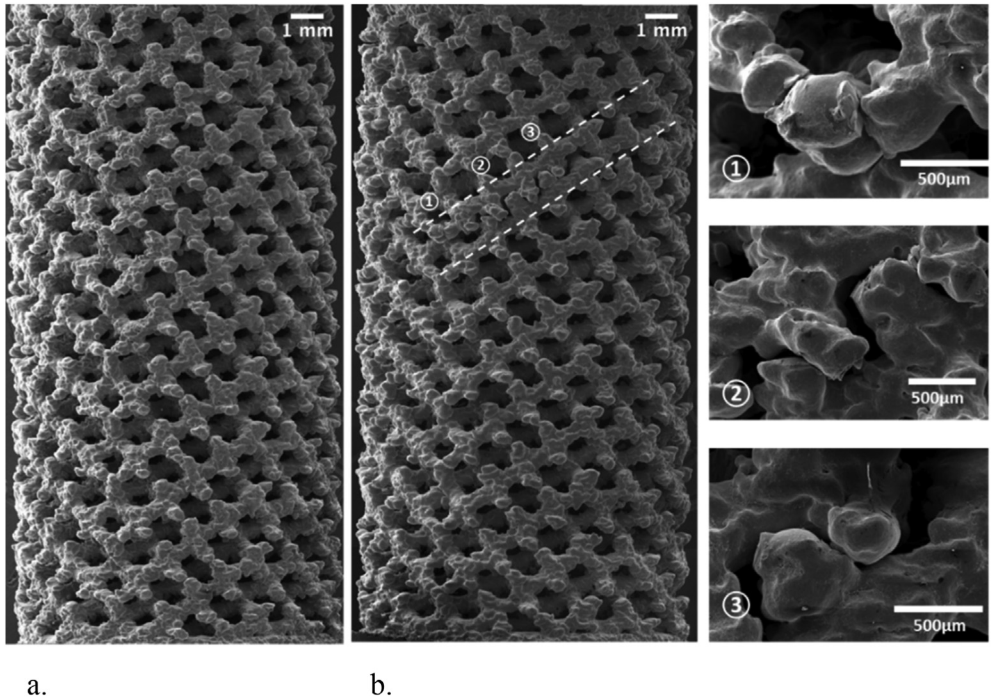

Fig. 5. SEM images of EBPBF [1 1 1] lattice samples, (a) before testing and (b) after testing displaying fracture along a raw (and plane behind) of the [1 1 1] struts.

deformation is yet to start. Thus, on average, the local effective diameter of the strut should increase, long before the strut to deform everywhere. This adds apparent hardening in the test curves due to the natural increase in diameter during compressive deformation. However, current simulation has not taken this into consideration. Thus, the apparent hardening is much more severe in the tested curves than the simulated curve. This high amount of apparent hardening is the effect of the geometrical irregularity, not the effect of the material property. This geometrical irregularity may also affect E_L in a similar way, with the experimental $E_{L\,[0\,0\,1]}$ underestimated.

For [1 1 1] lattices, there could be another effect of strut irregularity, in combination of stress distribution, on the mechanical behaviour. Fig. 4 shows the distribution of σ_1 from simulation at the time when the applied load reaches 7,695 N, meaning also that the applied stress is 98 MPa (=$\sigma_{y\text{-}L}$). At the same time, at or near the struts connecting nodes, σ_1 can be seen higher than 1,000 MPa (Fig. 4b), which is a high value as it is comparable to the yield strength of the alloy. For [0 0 1] lattices, as shown in Fig. 4a, at the same load, maximum σ_1 is only ~300 MPa. It can be shown that when the load has increased approximately 1.8 times, meaning that applied load is 13,500 N and $\sigma_{y\text{-}L}$ (=172 MPa) is reached, $\sigma_1 \approx 611$Mpa. This value is about a little over 60% of the yield strength of the alloy.

The high and positive σ_1 locally distributed in the [1 1 1] samples when the apparent yielding ($\sigma_{y\text{-}L}$) is reached should readily

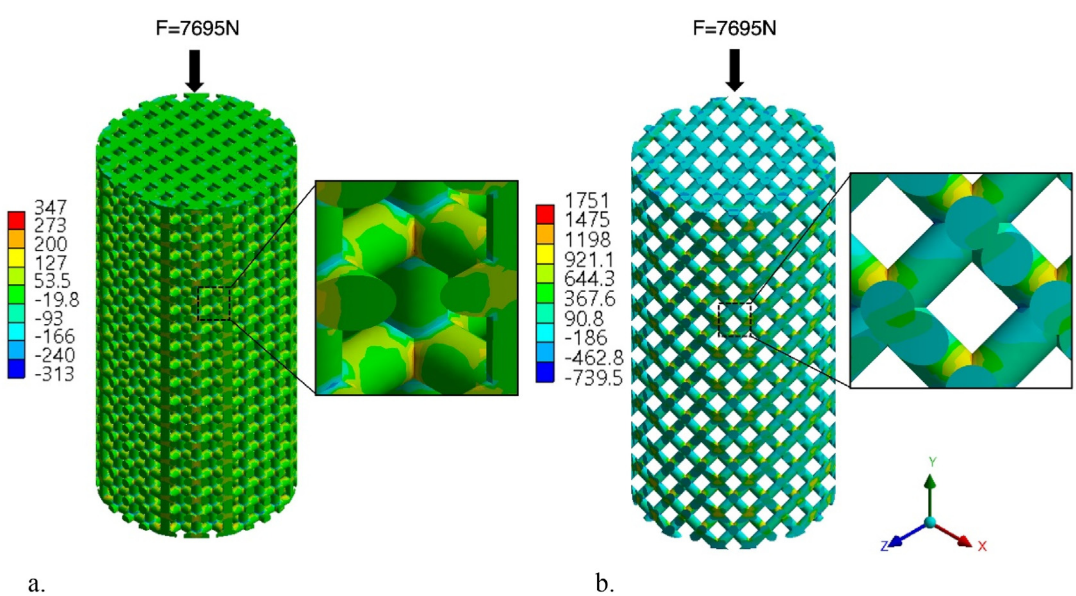

Fig. 4. Distribution of the maximum principal stress in (a) [0 0 1] and (b) [1 1 1] lattices.

cause the highly irregular struts to fail. Since there are a large number of locally sharp notches located in the highly irregular struts, acting as crack initiation sites, these locations under a high tensile stress should be the favourable locations for crack propagation. Thus, by the time the load is increased to the level corresponding to $\sigma_{y\text{-}L}$, fracturing of the lattice should occur. This is the reason why ε_p is only 0.011 for [1 1 1] lattices, while for [0 0 1] lattices, ε_p is high at 0.065. As is indicative in the experimental stress–strain curves in Fig. 2b, in each of the tests, the sample fractured, and the stress reduced soon after UCS_L. Fig. 5 shows a [1 1 1] lattice sample before test and a fractured [1 1 1] lattice sample. Collapsing by fracturing through a plane of struts globally and, locally, cracking of notched locations are evident in Fig. 5b. On the other hand, [0 0 1] samples started severely distorting when σ approached UCS_L but did not collapse (fracture) during testing.

4. Conclusions

Compressive strength of simple cubic unit cell based lattices is highly load orientation dependent. Experiments and simulations have both shown that the apparent yield strength ($\sigma_{y\text{-}L}$) of [0 0 1] lattices is 1.8 times higher than that of [1 1 1] lattices. EPPBF has resulted in an average strut size over 10% larger than the designed strut size. Thus, the experimentally determined $\sigma_{y\text{-}L}$ values are close to 10% higher than the value obtained by simulation. In the condition of loading in parallel to [0 0 1] ([0 0 1]//LD), the highly irregular struts with notches cause the effective strut size to increase during loading when locally the sharp notches close. Thus, the strain hardening is apparently higher in the experimental curves than that in the simulation curve. Simulation has shown that, with the [1 1 1]//LD condition, σ_1 is locally higher than 1,000 MPa and is positive when $\sigma_{y\text{-}L}$ is reached. This locally high stress level in tension together with the strut irregularity and a high number of notches suggests fracture should occur when $\sigma_{y\text{-}L}$ is reached. This suggestion is in a close agreement with experiments that compression plastic strain (ε_p) is low at 0.011. On the other hand, for the [0 0 1]//LD condition, compression loading causes the closure of notches experimentally and locally σ_1 is 30–40% lower than the yield stress of the alloy when $\sigma_{y\text{-}L}$ is reached. Thus, there is no mechanism for lattice fracturing and collapsing. The [0 0 1] lattices distort heavily when ultimate compressive stress (UCS_L) is reached with ε_p = 0.065.

Declaration of Competing Interest

The authors declare that they have no known competing financial interests or personal relationships that could have appeared to influence the work reported in this paper.

References

[1] Y. Lv, B. Wang, G. Liu, Y. Tang, E. Lu, K. Xie, C. Lan, J. Liu, Z. Qin, L. Wang, Metal Material, Properties and Design Methods of Porous Biomedical Scaffolds for Additive Manufacturing: A Review, Front. Bioeng. Biotechnol. 9 (2021).
[2] D. Barba, E. Alabort, B.C. Reed, Synthetic bone: Design by additive manufacturing, Acta Biomater. 97 (2019) 637–656.
[3] A.A. Zadpoor, Additive manufactured porous metallic biomaterials, J. Mater. Chem. B 7 (2019) 4088–4117.
[4] Z. Alomar, F. Concli, A Review of the selective laser melting lattice structures and their numerical models, Adv. Eng. Mater. 22 (2020) 2000611.
[5] M. McGregor, S. Patel, S. McLachlin, M. Vlasea, Architectural bone parameters and the relationship to titanium lattice design for powder bed fusion additive manufacturing, Addit. Manuf. 47 (2021).
[6] X.Z. Zhang, M. Leary, H.P. Tang, T. Song, M. Qian, Selective electron beam manufactured Ti-6Al-4V lattice structures for orthopedic implant applications: Current status and outstanding challenges, Curr. Opin. Solid State Mater. Sci. 22 (2018) 75–99.
[7] G. Del Guercio, M. Galati, A. Saboori, P. Fino, L. Iuliano, Microstructure and Mechanical Performance of Ti–6Al–4V Lattice Structures Manufactured via Electron Beam Melting (EBM): A Review, Acta Metall. Sin. (English Lett.) 33 (2020) 183–203.
[8] L.J. Gibson, M.F. Ashby, Cellular Solids: Structure and Properties, 2nd ed., Cambridge University Press, New York, 1999.
[9] T.J. Horn, O.L.A. Harrysson, D.J. Marcellin-Little, H.A. West, B.D.X. Lascelles, R. Aman, Flexural properties of Ti6Al4V rhombic dodecahedron open cellular structures fabricated with electron beam melting, Addit. Manuf. 1–4 (2014) 2–11.
[10] G. Del Guercio, M. Galati, A. Saboori, Innovative approach to evaluate the mechanical performance of Ti–6Al–4V lattice structures produced by electron beam melting process, Met. Mater. Int. 27 (2021) 55–67.
[11] G. Del Guercio, M. Galati, A. Saboori, Electron beam melting of Ti-6Al-4V lattice structures: correlation between post heat treatment and mechanical properties, Int. J. Adv. Manuf. Technol. 116 (2021) 3535–3547.